International Journal of Thermophysics, Vol. 25, No. 3, May 2004 (© 2004)

A Thermodynamic Property Model for Fluid Phase Hydrogen Sulfide

N. Sakoda[1,2] **and M. Uematsu**[1]

Received July 31, 2003

A Helmholtz free energy equation of state for the fluid phase of hydrogen sulfide has been developed as a function of reduced temperature and density with 23 terms on the basis of selected measurements of pressure–density–temperature (P, ρ, T), isobaric heat-capacity, and saturation properties. Based on a comparison with available experimental data, it is recognized that the model represents most of the reliable experimental data accurately in the range of validity covering temperatures from the triple point temperature (187.67 K) to 760 K at pressures up to 170 MPa. The uncertainty in density calculation of the present equation of state is 0.7% in the liquid phase, and that in pressure calculation is 0.3% in the vapor phase. The uncertainty in saturated vapor pressure calculation is 0.2%, and that in isobaric heat-capacity calculation is 1% in the liquid phase. The behavior of the isobaric heat-capacity, isochoric heat-capacity, speed-of-sound, and Joule–Thomson coefficients calculated by the present model shows physically reasonable behavior and those of the calculated ideal curves also illustrate the capability of extending the range of validity. Graphical and statistical comparisons between experimental data and the available thermodynamic models are also discussed.

KEY WORDS: equation of state; Helmholtz free energy; hydrogen sulfide; thermodynamic properties.

1. INTRODUCTION

Recent environmental problems have been considered globally. Yielding less harmful products than petroleum in combustion, natural gas has been

[1] Center for Mechanical Engineering and Applied Mechanics, Keio University, Hiyoshi 3-14-1, Kohoku-ku, Yokohama 223-8522, Japan.
[2] To whom correspondence should be addressed. E-mail: ud06599@educ.cc.keio.ac.jp

0195-928X/04/0500-0709/0

given attention and its thermophysical properties are required. Natural gas is a multicomponent system whose primary component is methane, and it is very difficult to predict the thermophysical properties of natural gas because the components are different depending on the source. Hydrogen sulfide is a component of natural gas. The behavior of hydrogen sulfide in natural gas is very interesting. Binary mixtures of methane and hydrogen sulfide show vapor–liquid–liquid equilibrium and divergence of its critical curve. Binary mixtures of ethane and hydrogen sulfide and those of propane and hydrogen sulfide show an azeotrope. But the thermophysical properties of hydrogen sulfide have not been studied enough until now. Starling [1] developed a BWR-type equation of state for 15 components of natural gas including hydrogen sulfide in 1973. The equation of state by Starling has a common functional form for these 15 pure fluids (methane, ethane, propane, *n*-butane, *i*-butane, *n*-pentane, *i*-pentane, *n*-hexane, *n*-heptane, *n*-octane, ethylene, propylene, carbon dioxide, hydrogen sulfide, and nitrogen). The valid temperature range is from 189 to 589 K at pressures up to 55 MPa for hydrogen sulfide. Goodwin [2] in 1983 surveyed the experimental data of hydrogen sulfide in detail and determined the thermophysical properties of hydrogen sulfide in the temperature range from 188 to 700 K at pressures up to 75 MPa. In 2001, Ihmels and Gmehling [3] presented 468 $P\rho T$ data with an uncertainty of 0.3% in density measurements covering a wide temperature range from gas to liquid phases including the supercritical-fluid region from 273 to 548 K at pressures up to 40 MPa. In this study we present an equation of state for hydrogen sulfide using the Helmholtz free energy function. Our objective in developing an equation of state for hydrogen sulfide was to make clear its effect on the behavior of natural gas.

2. SELECTION OF INPUT DATA

We compiled about 1600 experimental thermodynamic property measurements for hydrogen sulfide. A summary of the $P\rho T$ data, saturation property data including saturated vapor pressures, saturated vapor and liquid densities, and of the caloric property measurements is listed in Table I. Most of the experimental thermodynamic property data reported prior to 1983 were summarized by Goodwin [2]. For our modeling efforts, temperature values of all experimental data have been converted to ITS-90. The available experimental data for hydrogen sulfide are much fewer than those for other components of natural gas. There are few reliable caloric property data and no acoustic property data for hydrogen sulfide.

The distribution of the single-phase $P\rho T$ data on a pressure–temperature plane is shown in Fig. 1. Reamer et al. [5] first measured $P\rho T$ data

Table I. Sources of Experimental Thermodynamic Property Data for Hydrogen Sulfide

				P		ρ		T	
Author [a,b]	Year	property	No. of Data	Range (MPa)	δP (kPa)	Range ($\text{mol}\cdot\text{dm}^{-3}$)	$\delta\rho$ ($\text{mol}\cdot\text{dm}^{-3}$)	Range (K)	δT (mK)
Wright and Maass [4]	1931	$P\rho T$	54	0.03 – 0.4	n.a.	0.01 – 0.2	n.a.	238 – 320	n.a.
Reamer et al. [5]	1950	$P\rho T$	275	0.1 – 69	0.05%	0.03 – 27	n.a.	278 – 444	n.a.
Lewis and Fredericks [6]	1968	$P\rho T$	106	9.1 – 171	0.25%	8.0 – 23	n.a.	373 – 493	500
Rau and Mathia [7]	1982	$P\rho T$	67	6.0 – 60	n.a.	3.0 – 15	n.a.	342 – 760	n.a.
Straty * [8]	1983	$P\rho T$	112	0.2 – 38	n.a.	0.05 – 13	n.a.	493 – 523	n.a.
Liu et al. [9]	1986	$P\rho T$	106	1.0 – 33	0.01%	0.24 – 19	1 %	300 – 500	10
Bailey et al. [10]	1987	$P\rho T$	86	0.2 – 33	0.1%	0.05 – 19	1 %	284 – 501	10
Ihmels and Gmehling * [3]	2001	$P\rho T$	468	2.8 – 40	6 kPa	2.4 – 26	0.3%	273 – 548	30
Cardoso [11]	1921	P_s	16	1.0 – 9.0	n.a.			273 – 373	n.a.
Klemenc and Bankowski [12]	1932	P_s	9	0.02 – 0.1	n.a.			188 – 213	n.a.
Giauque and Blue * [13]	1936	P_s	11	0.02 – 0.1	n.a.			188 – 213	n.a.
Reamer et al. * [5]	1950	P_s	21	1.2 – 9.0	0.05%			278 – 374	n.a.
Clark et al. # [14]	1951	P_s	8	0.02 – 0.14	n.a.			188 – 220	50
Bierlein and Kay [15]	1953	P_s	16	1.5 – 9.0	0.1%			286 – 374	20
Kay and Brice [16]	1953	P_s	9	1.4 – 8.9	n.a.			283 – 373	n.a.
Kay and Rambosek [17]	1953	P_s	31	1.0 – 8.9	0.7 kPa			272 – 373	n.a.
Reamer et al. [18]	1953	P_s	4	1.2 – 9.0	0.1%			278 – 373	20
Clarke and Glew * [19]	1970	P_s	26	0.04 – 2.3	0.03%			195 – 303	n.a.
Reamer et al. [5]	1950	ρ^V	16			0.6 – 10	n.a.	278 – 374	n.a.
Bierlein and Kay [15]	1953	ρ^V	16			0.8 – 10	0.5 %	286 – 374	20

Table I. *(Continued)*

Author [a,b]	Year	Property	No. of Data	P Range (MPa)	P δP (kPa)	ρ Range ($mol \cdot dm^{-3}$)	ρ $\delta\rho$ ($mol \cdot dm^{-3}$)	T Range (K)	T δT (mK)
Kay and Rambosek [17]	1953	ρ^V	13			1.4 – 10	0.004	311 – 373	n.a.
Reamer et al. [18]	1953	ρ^V	4			0.6 – 10	0.25%	278 – 373	20
Clarke and Glew *, # [19]	1970	ρ^V	29			0.02 – 1.8	n.a.	193 – 323	n.a.
Klemenc and Bankowski * [12]	1932	ρ^L	12			27.9 – 29.0	n.a.	190 – 212	n.a.
Baxter et al. [20]	1934	ρ^L	7			20.0 – 27.5	n.a.	192 – 331	n.a.
Reamer et al. * [5]	1950	ρ^L	16			10.2 – 24.2	n.a.	278 – 374	n.a.
Bierlein and Kay [15]	1953	ρ^L	16			10.2 – 23.9	0.5%	286 – 374	20
Kay and Rambosek [17]	1953	ρ^L	20			10.2 – 25.0	0.04	272 – 373	n.a.
Reamer et al. [18]	1953	ρ^L	4			10.2 – 24.2	0.25%	278 – 373	20
Clarke and Glew * [19]	1970	ρ^L	30			20.9 – 28.9	n.a.	193 – 323	n.a.
Cubitt et al. [21]	1987	ρ^L	18			25.1 – 28.7	n.a.	197 – 265	n.a.
Millar [22]	1923	C_P	5	0.1	n.a.			216 – 278	n.a.
Clusius and Frank [23]	1936	C_P	4					194 – 209	n.a.
Giauque and Blue * [13]	1936	C_P	6					189 – 211	n.a.
Swamy and Rao # [24]	1970	C_P	6					188 – 213	n.a.
Millar # [22]	1923	C_V	5	0.1	n.a.			216 – 278	n.a.
Swamy and Rao # [24]	1970	C_V	6					188 – 213	n.a.

[a] Data used as input data are denoted by *.
[b] Calculated data are denoted by #.

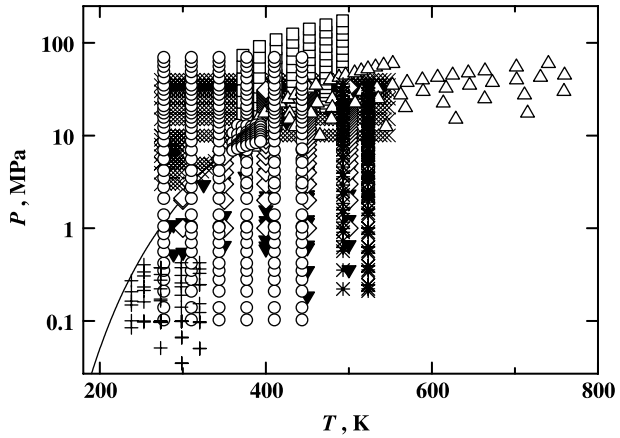

Fig. 1. Distribution of experimental $P\rho T$ data. (+) Wright and Maass [4], (◯) Reamer et al. [5], (□) Lewis and Fredericks [6], (△) Rau and Mathia [7], (∗) Straty [8], (◇) Liu et al. [9], (▼) Bailey et al. [10], (×) Ihmels and Gmehling [3].

in the compressed liquid region from 278 to 444 K at pressures to 69 MPa in 1950. They used mercury to measure densities and stated in their report that hydrogen sulfide reacts with mercury to form hydrogen. Goodwin [2] considered that some of the data of Reamer et al. [5] seemed to be unreliable. Lewis and Fredericks [6] in 1968 measured $P\rho T$ data covering the high-pressure region to 170 MPa from 373 to 493 K. Rau and Mathia [7] in 1982 measured $P\rho T$ data in the high-temperature region from 342 to 760 K at pressures to 60 MPa. Goodwin [2] used the $P\rho T$ data of Reamer et al. [5] and those of Straty [8] which cover the gas-phase region from 493 to 523 K as input data for developing his equation of state. Liu et al. [9] in 1986 measured $P\rho T$ data in the temperature range from 300 to 500 K at pressures to 33 MPa. Bailey et al. [10] in 1987 measured $P\rho T$ data in the temperature range from 284 to 501 K at pressures to 33 MPa. In 2001, Ihmels and Gmehling [3] measured $P\rho T$ data over the wide range of temperatures from 273 to 548 K at pressures from 2.8 to 40 MPa and presented 468 measurements. In this study we used $P\rho T$ data of Straty [8] and those of Ihmels and Gmehling [3] as input data for developing our equation of state. These two data sets are indicated with superscript asterisks in Table I. Other sets of $P\rho T$ data were used only to compare with our formulation.

The distribution of saturated vapor pressures is shown in Fig. 2, and those of saturated vapor and liquid densities are shown in Fig. 3. Goodwin [2] stated in his report that the work of Clarke and Glew [19] is especially valuable. The saturation property data used for our modeling were

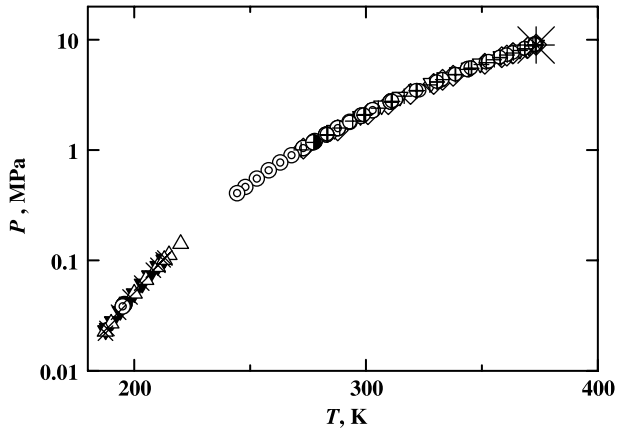

Fig. 2. Distribution of experimental data for the saturated vapor pressure. (◇) Cardoso [11], (×) Klemenc and Bankowski [12], (▼) Giauque and Blue [13], (◯) Reamer et al. [5], (△) Clark et al. [14], (▽) Bierlein and Kay [15], (⊕) Kay and Brice [16], (+) Kay and Rambosek [17], (◑) Reamer et al. [18], (◎) Clarke and Glew [19], (⁎) Critical point.

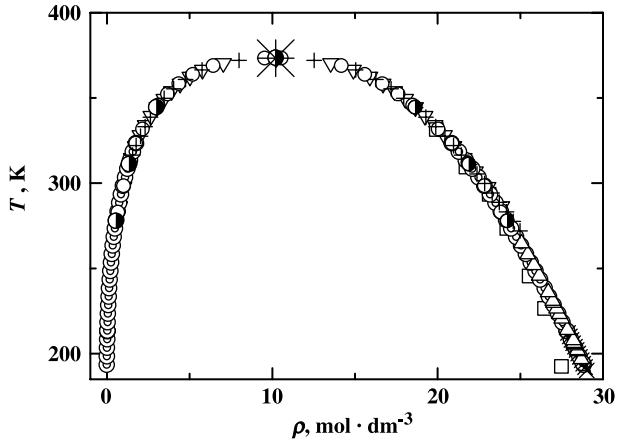

Fig. 3. Distribution of experimental data for the saturated vapor and liquid density. (×) Klemenc and Bankowski [12], (□) Baxter et al. [20], (◯) Reamer et al. [5], (▽) Bierlein and Kay [15], (+) Kay and Rambosek [17], (◑) Reamer et al. [18], (◎) Clarke and Glew [19], (△) Cubitt et al. [21], (⁎) Critical point.

determined according to the selection by Goodwin and are also indicated with superscript asterisks in Table I. These selected data were used to provide ancillary correlations discussed in the next section.

As shown in Table I, there are few caloric property data for hydrogen sulfide. Millar [22] presented five experimental isobaric heat-capacities, C_P, in the temperature range from 216 to 278 K at 0.1 MPa in 1923. He calculated five isochoric heat-capacities, C_V, with the use of these experimental isobaric heat-capacities. Clusius and Frank [23] presented four experimental isobaric heat-capacity data of the saturated liquid in the temperature range from 194 to 209 K in 1936. Giauque and Blue [13] also presented six experimental isobaric heat-capacity data of the saturated liquid in the temperature range from 189 to 211 K in 1936. In 1970, Swamy and Rao [24] calculated six isobaric heat-capacities and six isochoric heat-capacities of the saturated liquid in the temperature range from 188 to 213 K. They compared their calculated data with the experimental data by Giauque and Blue [13]. Their values are larger than those of Giauque and Blue with the largest deviation reaching 16%. The isobaric heat-capacity data of the saturated liquid by Giauque and Blue were used as input data. The reliability of their measurements is indicated from the result that the isobaric heat-capacity data for nitrogen by Giauque and Clayton [25] in 1933 are in good agreement with the values calculated by the reference equation of state developed by Span et al. [26].

Ideal-gas heat-capacity data for hydrogen sulfide are listed in Table II. Most of the isobaric heat-capacity data were calculated on the basis of spectroscopic data. However, Millar [22] calculated the ideal heat-capacities using their experimental isobaric heat-capacities and Felsing and Drake [28] measured the gaseous heat-capacities in the temperature range from 303 to 383 K. Goodwin correlated the ideal heat-capacities of Baehr et al. [32]. In 1995, Jaeschke and Schley [35] presented ideal-gas heat-capacity correlations for 19 components of natural gas. They used the data of JANAF [33] between 100 and 1000 K for hydrogen sulfide, and their model represents these data within $\pm 0.02\%$.

A summary of reported critical parameter values is given in Table III. For our modeling, the values of the critical temperature, density, and pressure determined by Goodwin [2] with the use of law of rectilinear diameters are adopted. Jou et al. [37] in 1995 measured the critical temperatures and pressures for the binary mixtures of propane and hydrogen sulfide and they stated that the critical parameters by Goodwin [2] are believed to be the best values for hydrogen sulfide. The experimental critical temperature of Jou et al., which was determined by observation of the disappearance of the meniscus, agrees with the value of Goodwin [2] within their reported uncertainty. In this study, the values of triple point temperature and normal boiling temperature given by Goodwin are also adopted and these values are, respectively, 187.67 and 218.88 K, which are converted to ITS-90.

Table II. Sources of Ideal-Gas Isobaric Heat-Capacity Data for Hydrogen Sulfide

Author	Year	Number of data	Temperature Range T (K)
Millar [22]	1923	5	216 – 278
Cross [27]	1935	17	213 – 1800
Felsing and Drake [28]	1936	3	303 – 383
Barrow and Pitzer [29]	1949	8	298 – 1000
Evans and Wagman [30]	1952	14	298 – 1500
McBride and Gordon [31]	1961	42	100 – 6000
Baehr et al. [32]	1968	48	50 – 1300
JANAF [33]	1985	61	100 – 6000
TRC [34]	1993	29	50 – 5000

Table III. Summary of Available Critical Parameters for Hydrogen Sulfide[a,b]

Author	Year	Method[c]	T_c (K)	P_c (MPa)	ρ_c (mol·dm^{-3})
Cardoso and Arni [36]	1912	1	373.37	9.023	–
Cardoso [11]	1921	1	373.37	9.008	–
Reamer et al. [5]	1950	2	373.51	9.005	10.23
Bierlein and Kay [15]	1953	2	373.50	9.005	10.24
Kay and Brice [16]	1953	2	373.05	8.943	10.17
Kay and Rambosek [17]	1953	2	373.05	8.943	10.17
Reamer et al. [18]	1953	2	373.29	9.005	10.23
Goodwin [2]	1983	3	373.37*	8.96291*	10.20*
Jou et al. [37]	1995	1	373.45	9.000	–
Guilbot et al. [38]	2000	1	372.78	8.938	–

[a] All temperature values in this table were converted to ITS–90.
[b] Critical parameter values used for our modeling are denoted by *.
[c] Method of decision of critical parameter was classified by three ways shown below.
1. Observation of the meniscus.
2. Pressure–volume–temperature relations: $(\partial P/\partial \rho) = 0$.
3. Law of rectilinear diameters.

3. ANCILLARY CORRELATIONS

It is usually difficult to measure $P\rho T$ data at low pressures in the vapor phase. Therefore, we prepared a set of supplementary input $P\rho T$ data for modeling at low pressures in the vapor phase which were calculated from the virial equation of state given in the following equation.

$$\frac{P}{\rho RT} = 1 + \left[A_1 + A_2 T_r^{-1} + A_3 \exp(T_r^{-1})\right]\rho + \left[A_4 + A_5 T_r^{-5} + A_6 T_r^{-12}\right]\rho^2 + A_7 T_r^{-2.25}\rho^3 \quad (1)$$

Table IV. Coefficients in Eqs. (1)–(4)

i	A_i	B_i	C_i	D_i
1	0.1973031	−6.423889	−2.001663	2.122841
2	−0.1594372	1.699405	−3.339645	−0.8907727
3	−0.0570357	−1.211219	−0.6781599	0.1148276
4	0.0066157	−2.217591	−13.33131	
5	0.0072839		−3.988066	
6	−0.0000702		−75.23041	
7	−0.0042857			

where P denotes the pressure in MPa, T is the temperature in K, ρ is the density in $\text{mol} \cdot \text{dm}^{-3}$, and R is the universal gas constant, $R = 8.314472\,\text{J} \cdot \text{mol}^{-1} \cdot \text{K}^{-1}$ [39]. The reduced temperature $T_r = T/T_c$ is reduced by the critical temperature, $T_c = 373.37$ K. Equation (1) has been developed on the basis of the $P\rho T$ data in the vapor phase below the critical temperature of Wright and Maass [4] and of Reamer et al. [5]. The equation with the coefficients in Table IV represents these experimental data within $\pm 0.5\%$ in pressure except in the region near the critical point and the saturation boundary.

In this study, the following three ancillary correlations for the saturation properties (P_S: saturated vapor pressure, ρ^V: saturated vapor density, and ρ^L: saturated liquid density) were developed on the basis of the selected experimental data indicated with superscript asterisks in Table I.

$$\ln \frac{P_S}{P_c} = \frac{1}{1-x}\left(B_1 x + B_2 x^{1.5} + B_3 x^2 + B_4 x^{4.5}\right) \tag{2}$$

$$\ln \frac{\rho^V}{\rho_c} = C_1 x^{0.354} + C_2 x^{5/6} + C_3 x^{3/2} + C_4 x^{5/2} + C_5 x^{25/6} + C_6 x^{47/6} \tag{3}$$

$$\ln \frac{\rho^L}{\rho_c} = D_1 x^{0.354} + D_2 x^{1/2} + D_3 x^{5/2} \tag{4}$$

where P_c is the critical pressure, 8.96291 MPa, $x = 1 - T/T_c$, and ρ_c is the critical density, 10.20 $\text{mol} \cdot \text{dm}^{-3}$. The coefficients in Eqs. (2)–(4) are listed in Table IV. The saturation property data calculated by Eqs. (2)–(4) were used as sets of supplementary input data for the present modeling.

4. FUNDAMENTAL EQUATION OF STATE

On the basis of the experimental $P\rho T$ data of Straty [8] and Ihmels and Gmehling [3], and the isobaric heat-capacity data of the saturated liquid by Giauque and Blue [13] in addition to sets of supplementary saturation data, we formulated an equation of state for hydrogen sulfide. The equation is expressed using the Helmholtz free energy, a, as a function of

temperature and density in dimensionless form. Our model of the reduced Helmholtz free energy, $\phi(\tau, \delta)$, given in Eq. (5) consists of the ideal-gas state contribution, $\phi^0(\tau, \delta)$, expressed by Eq. (6), and the residual real fluid contribution, $\phi^r(\tau, \delta)$, by Eq. (7).

$$\phi(\tau, \delta) = \frac{a}{RT} = \phi^0(\tau, \delta) + \phi^r(\tau, \delta) \tag{5}$$

$$\phi^0(\tau, \delta) = \ln(\delta) + f_1 + f_2\tau + f_3 \ln(\tau) + \sum_{i=4}^{5} f_i \ln\left\{1 - \exp\left(-g_i\tau\right)\right\} \tag{6}$$

$$\begin{aligned}\phi^r(\tau, \delta) = &\sum_{i=1}^{11} n_i \tau^{t_i} \delta^{d_i} + \sum_{i=12}^{16} n_i \tau^{t_i} \delta^{d_i} \exp(-\delta) + \sum_{i=17}^{19} n_i \tau^{t_i} \delta^{d_i} \exp\left(-\delta^2\right) \\ &+ \sum_{i=20}^{21} n_i \tau^{t_i} \delta^{d_i} \exp\left(-\delta^3\right) + \sum_{i=22}^{23} n_i \tau^{t_i} \delta^{d_i} \exp\left(-\delta^4\right)\end{aligned} \tag{7}$$

where $\tau = T_c/T$ is the inverse reduced temperature and $\delta = \rho/\rho_c$ is the reduced density. The coefficients for Eqs. (6) and (7) are listed in Tables V and VI, respectively. The ideal-gas part of the present equation of state, Eq. (6), is developed from the ideal-gas heat-capacity correlation by Jaeschke and Schley [35] and was fitted to the values calculated from their correlation. In the course of the development of the formulation, it was found that the $P\rho T$ data of Ihmels and Gmehling in the vapor phase deviate systematically from those of Straty and the extrapolations of Ihmels and Gmehling to the saturated liquid state are not consistent with the saturated liquid densities calculated by Eq. (4). Here, the $P\rho T$ data of Straty in the vapor phase and those of Ihmels and Gmehling in the liquid phase were used as input data. Backward regression analysis and nonlinear fitting of n_i and t_i were applied to the present formulation. The final form of Eq. (7) is expressed with 23 terms. The molar entropy is given a value of zero at 298.15 K and 0.1 MPa in the ideal-gas state, and the molar enthalpy is given a value of zero at 298.15 K in the ideal-gas state.

Table V. Coefficients in Eq. (6)

i	f_i	g_i
1	7.881037	–
2	−3.209860	–
3	3.000000	–
4	0.9767422	4.506266
5	2.151898	10.15526

Table VI. Coefficients in Eq. (7)

i	n_i	d_i	t_i
1	0.1545780×10^{0}	1	0.241
2	-0.1717693×10^{1}	1	0.705
3	-0.1595211×10^{1}	1	1.000
4	0.2046589×10^{1}	2	0.626
5	-0.1690358×10^{1}	2	1.120
6	0.9483623×10^{0}	2	1.630
7	$-0.6800772 \times 10^{-1}$	3	0.210
8	0.4372273×10^{-2}	4	3.080
9	0.3788552×10^{-4}	8	0.827
10	$-0.3680980 \times 10^{-4}$	9	3.050
11	0.8710726×10^{-5}	10	3.050
12	0.6886876×10^{0}	1	0.110
13	0.2751922×10^{1}	1	1.070
14	-0.1492558×10^{1}	1	1.950
15	0.9202832×10^{0}	2	0.142
16	-0.2103469×10^{0}	5	2.130
17	0.1084359×10^{-2}	1	4.920
18	0.3754723×10^{-1}	4	1.750
19	$-0.5885793 \times 10^{-1}$	4	3.970
20	$-0.2329265 \times 10^{-1}$	3	11.800
21	$-0.1272600 \times 10^{-3}$	8	10.000
22	$-0.1336824 \times 10^{-1}$	2	9.830
23	0.1053057×10^{-1}	3	14.200

5. COMPARISONS WITH EXPERIMENTAL DATA

5.1. Ideal-Gas State

Figure 4 shows the deviations of the available ideal-gas heat-capacity data from corresponding values calculated by the present model at temperatures to 1000 K. In the upper figure, deviations from -1 to $+1\%$ are plotted; whereas in the lower figure, they are from -0.1 to $+0.1\%$. The present model is in good agreement with the correlation by Jaeschke and Schley [35] within $\pm 0.02\%$ and with the data of JANAF [33] within $\pm 0.02\%$. Deviations of Baehr et al. [32] as well as McBride and Gordon [31] increase to 0.3% at 1000 K with increasing temperature. The data of TRC [34] deviate from the present model within 1.9%. The data of Cross [27] are smaller than the present model with a maximum deviation of -0.8%, whereas those of Evans and Wagman [30] are larger with a maximum deviation of $+0.6\%$. The data of Barrow and Pitzer [29], those of Felsing and Drake [28], and those of Millar [22] deviate greatly from the present model. The Goodwin model, formulated based on the correlation

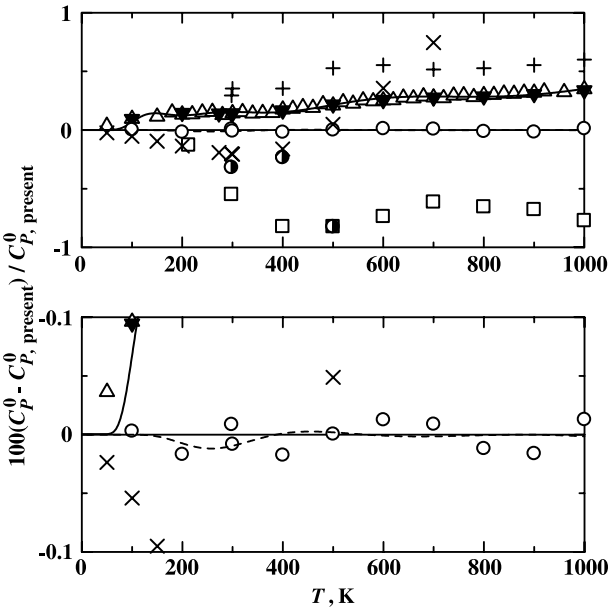

Fig. 4. Deviations of ideal-gas heat-capacities C_P^0 from the present model. (□) Cross [27], (◑) Barrow and Pitzer [29], (+) Evans and Wagman [30], (▼) McBride and Gorden [31], (△) Baehr et al. [32], (◯) JANAF [33], (×) TRC [34], (- - - - -) Jaeschke and Schley [35], (———) Goodwin [2].

by Baehr et al. [32] gives values larger than the present model by 0.1 to 0.3%.

5.2. $P\rho T$ Property Comparisons

Figures 5 and 6 show pressure deviations of the available $P\rho T$ measurements in the vapor phase from the present model. Here, the vapor phase covers densities smaller than the critical density, whereas the liquid phase includes densities larger than the critical density. Figure 5 covers temperatures below the critical temperature, and Fig. 6 covers those above the critical temperature. The $P\rho T$ data of Wright and Maass [4] cover the range of temperatures from 238 to 320 K at pressures from 0.03 to 0.4 MPa. Our model satisfactorily represents these data with pressure deviations from −0.13 to + 0.26%. The data of Reamer et al. [5], which are represented with pressure deviations from −1.2 to + 1.4%, cover the range of temperatures from 278 to 444 K and pressures from 0.1 to

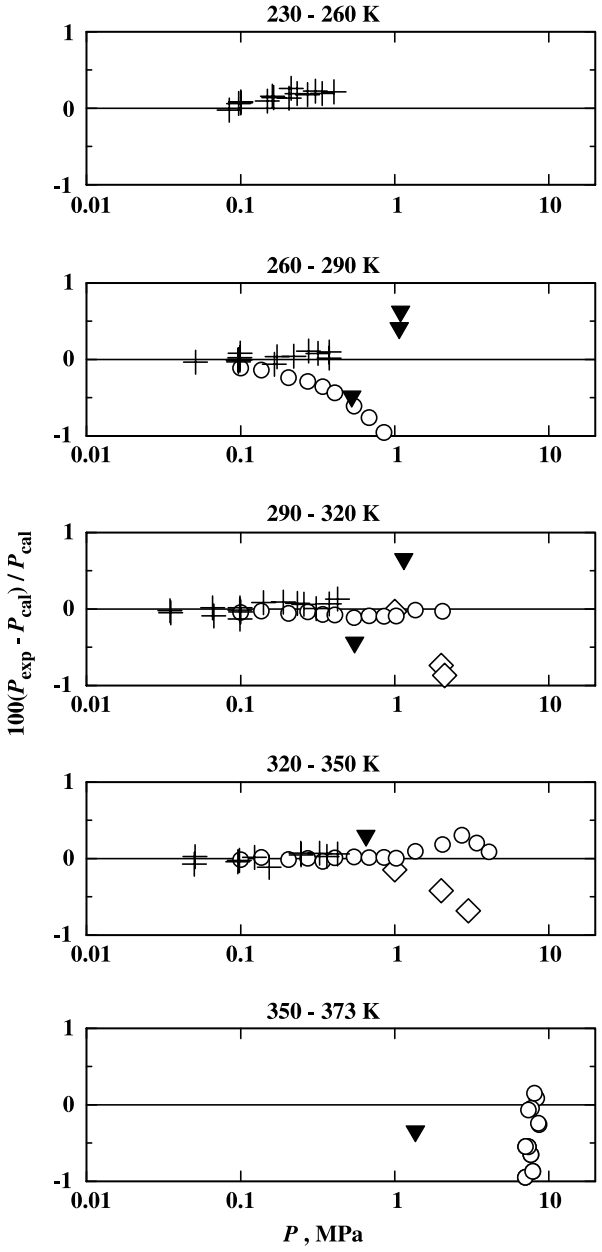

Fig. 5. Pressure deviations of $P\rho T$ data from the present model below T_c in the vapor phase. (+) Wright and Maass [4], (○) Reamer et al. [5], (□) Lewis and Fredericks [6], (◇) Liu et al. [9], (▼) Bailey et al. [10].

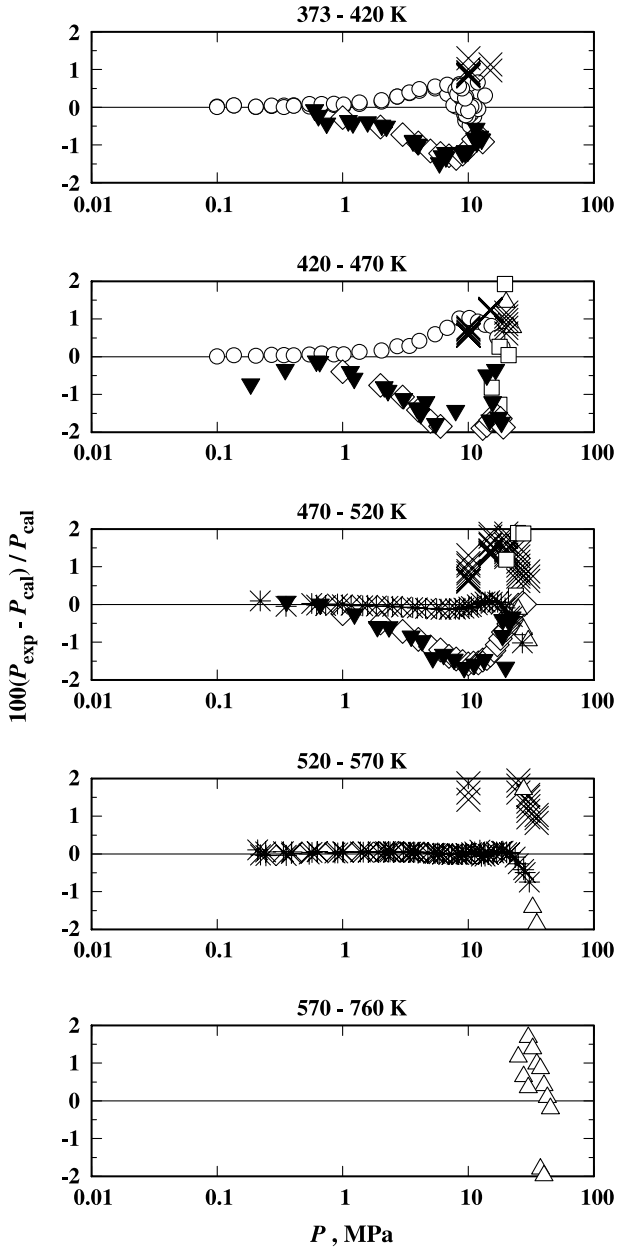

Fig. 6. Pressure deviations of $P\rho T$ data from the present model above T_c in the vapor phase. (◯) Reamer et al. [5], (□) Lewis and Fredericks [6], (△) Rau and Mathia [7], (∗) Straty [8], (◇) Liu et al. [9], (▼) Bailey et al. [10], (×) Ihmels and Gmehling [3].

19 MPa. These deviations increase with increasing pressure. The data of Rau and Mathia [7] covering the range of temperatures from 342 to 760 K and pressures from 6.0 to 60.0 MPa deviate significantly from our model by −3.6 to +11.7%. The data of Lewis and Fredericks [6] also deviate significantly from the present model within ± 7.8% and cover the range of temperatures from 393 to 493 K and pressures from 10 to 28 MPa. The data of Liu et al. [9] cover the range of temperatures from 300 to 500 K and pressures from 1.0 to 28 MPa. The data of Bailey et al. [10] cover the range of temperatures from 284 to 501 K and pressures from 0.2 to 22 MPa. Liu et al. and Bailey et al. are from the same research group, and their deviations from the present model show a similar tendency. The present model represents most of their data within ± 2.2%. The data of Straty [8] cover the range of temperatures from 493 to 523 K at pressures up to 31 MPa. The present model satisfactorily represents their data within ± 0.2% at pressures up to 20 MPa, but above this pressure the deviations increase with pressure and reach a maximum of −2.2%. Figure 6 shows that the data of Ihmels and Gmehling [3] are systematically larger in pressure than those of Straty by about 1–3%. The data of Ihmels and Gmehling [3] cover the range of temperatures from 383 to 548 K and of pressures from 10 to 35 MPa. The present model shows systematic deviations from these data, and the maximum pressure deviation reaches 3.0%.

Figures 7 and 8 show density deviations of the available $P\rho T$ measurements in the liquid phase from the present model. Figure 7 covers the region below the critical temperature, and Fig. 8 covers the region above the critical temperature. The present model represents the $P\rho T$ data of Ihmels and Gmehling [3] with density deviations from −4.8 to + 0.22% except for some data points in the region near the critical point. These data cover the range of temperatures from 274 to 548 K at pressures up to 40 MPa. As we mentioned above, the extrapolations of Ihmels and Gmehling to the saturated liquid state are not consistent with the saturated liquid densities and the deviations near the saturated liquid region tend to be larger. The data of Straty [8] covering the range of temperatures from 493 to 523 K at pressures up to 38 MPa in the liquid phase are systematically larger than those of Ihmels and Gmehling by about 2%. The data of Rau and Mathia [7] cover the range of temperatures from 380 to 553 K at pressures up to 60 MPa. Their deviations from the present model are in the range from −3.3 to +2.5%. Lewis and Fredericks [6] measured $P\rho T$ data in the range of temperatures from 373 to 493 K at pressures up to 171 MPa, and their data are represented by the present model with deviations from −2.0 to +16%. However, the present model is in good agreement with their data within ± 1.0% in the high-pressure region over 50 MPa. The data of Reamer et al. [5]

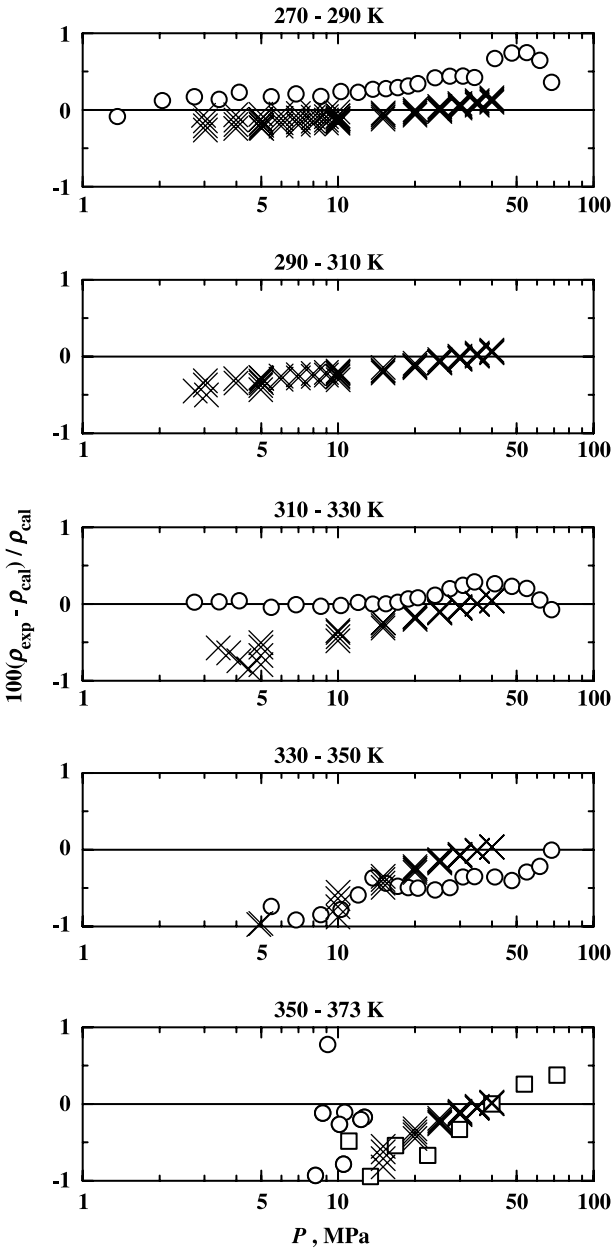

Fig. 7. Density deviations of $P\rho T$ data from the present model below T_c in the liquid phase. (○) Reamer et al. [5], (□) Lewis and Fredericks [6], (×) Ihmels and Gmehling [3].

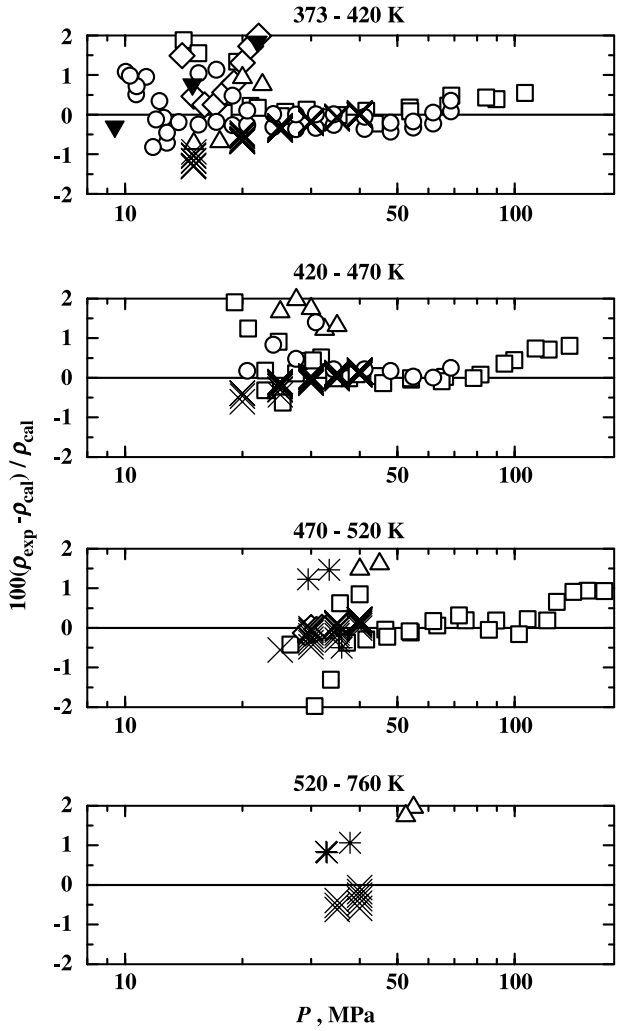

Fig. 8. Density deviations of $P\rho T$ data from the present model above T_c in the liquid phase. (○) Reamer et al. [5], (□) Lewis and Fredericks [6], (△) Rau and Mathia [7], (∗) Straty [8], (◇) Liu et al. [9], (▼) Bailey et al. [10], (×) Ihmels and Gmehling [3].

cover the range of temperatures from 278 to 444 K at pressures up to 69 MPa. The present model describes their data with deviations from −2.4 to + 2.0%.

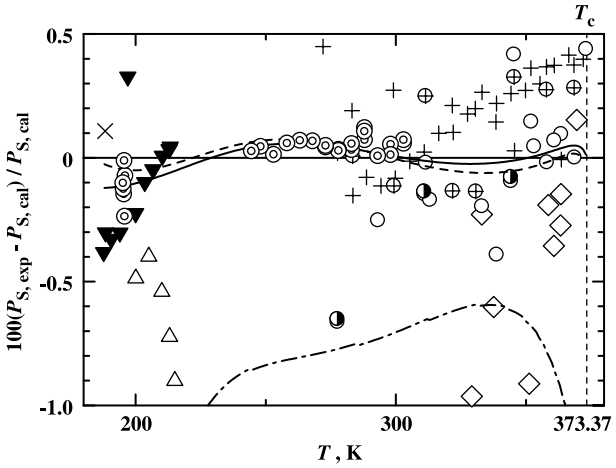

Fig. 9. Deviations of measured and calculated vapor-pressure values from the present model. (◇) Cardoso [11], (×) Klemenc and Bankowski [12], (▼) Giauque and Blue [13], (◯) Reamer et al. [5], (△) Clark et al. [14], (⊕) Kay and Brice [16], (+) Kay and Rambosek [17], (◑) Reamer et al. [18], (◎) Clarke and Glew [19], (–·–·–·) Starling model [1], (- - - - - -) Goodwin model [2], (———) Eq. (2).

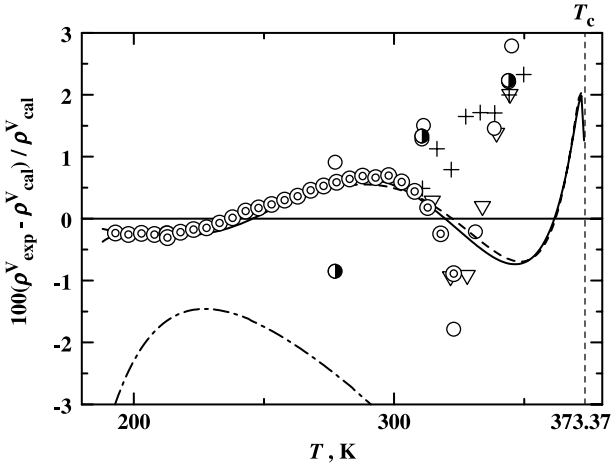

Fig. 10. Deviations of measured and calculated saturated vapor densities from the present model. (◯) Reamer et al. [5], (▽) Bierlein and Kay [15], (+) Kay and Rambosek [17], (◑) Reamer et al. [18] (◎) Clarke and Glew [19], (–·–·–·) Starling model [1], (- - - - - - -) Goodwin model [2], (———) Eq. (3).

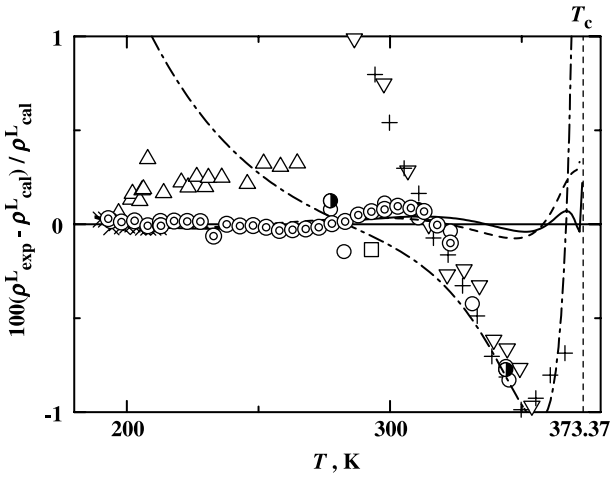

Fig. 11. Deviations of measured and calculated saturated liquid densities from the present model. (×) Klemenc and Bankowski [12], (□) Baxter et al. [20], (○) Reamer et al. [5], (▽) Bierlein and Kay [15], (+) Kay and Rambosek [17], (◑) Reamer et al. [18], (◎) Clarke and Glew [19], (△) Cubitt et al. [21], (–·–·–·–) Starling model [1], (- - - - - -) Goodwin model [2], (———) Eq. (4).

5.3. Saturation-Property Comparison

Deviations of thermodynamic properties along the saturation boundary from the present model are shown in Figs. 9–11. Figure 9 shows deviations of the saturated vapor pressure. The present model represents the saturated vapor-pressure measurements by Clarke and Glew [19] within ±0.25% and by Giauque and Blue [13] within ±0.4%. Figure 10 shows deviations of saturated vapor densities. The present model represents the saturated vapor density data calculated by Clarke and Glew [19] within ±1.0%. Figure 11 shows deviations of saturated liquid densities. The present model represents the saturated liquid-density data calculated by Clarke and Glew [19] within ±0.2% and the saturated liquid-density measurements by Cubitt et al. [21] within 0.06–0.35%. The calculated values from the ancillary correlation, Eq. (2), for the saturated vapor pressure and those from Eq. (4) for the saturated liquid density agree with the present model within ±0.2%. Equation (3) for the saturated vapor density deviates from the present model within ±1% except for the calculated values close to the critical temperature.

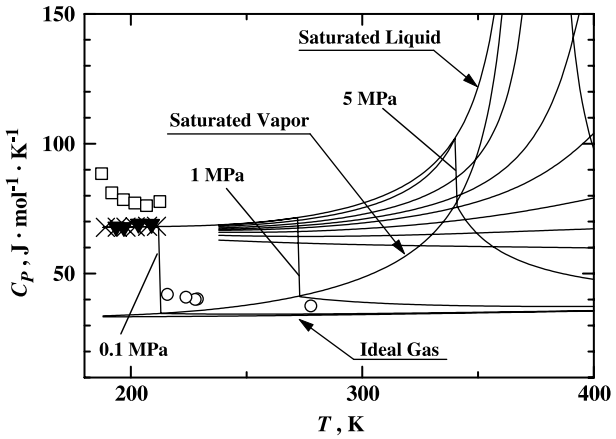

Fig. 12. Behavior of the isobaric heat-capacity calculated from the present model in the low temperature region with the available experimental data. (○) Millar [22], (▼) Clusius and Frank [23], (×) Giauque and Blue [13], (□) Swamy and Rao [24].

5.4. Caloric-Property Comparison

Figure 12 shows the behavior of the isobaric heat-capacity calculated from the present model in the low temperature region and the available experimental data. The present model is in good agreement with data of Giauque and Blue [13] and those of Clusius and Frank [23]. Figure 13 shows deviation plots of the experimental isobaric heat-capacity data of Giauque and Blue and those of Clusius and Frank from the present model. The deviations of the data of Giauque and Blue are within $\pm 0.3\%$, and those of Clusius and Frank are within $\pm 2\%$. There are large deviations with the data of Millar [22] and those of Swamy and Rao [24] as shown in Fig. 12. The isobaric heat-capacity data calculated by Swamy and Rao are larger than the present model by 11–19%. The deviations of the data of Millar from the present model are from 8 to 21%.

Figure 14 shows the behavior of the isochoric heat-capacity calculated from the present model in the low temperature region with the available experimental data. The deviations of the data of Millar [22] from the present model are from 11 to 27%. The isochoric heat-capacity data of Swamy and Rao [24] are also larger than the present model by 14–17%.

The Δh calculated by the present model at the normal boiling point temperature in terms of the Clausius–Clapeyron equation, Eq. (8),

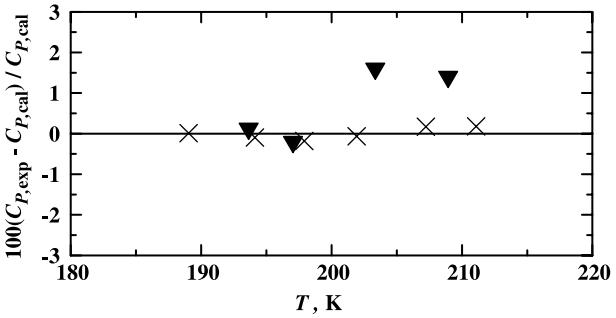

Fig. 13. Deviations of the isobaric heat-capacity data from the present model. (▼) Clusius and Frank [23], (×) Giauque and Blue [13].

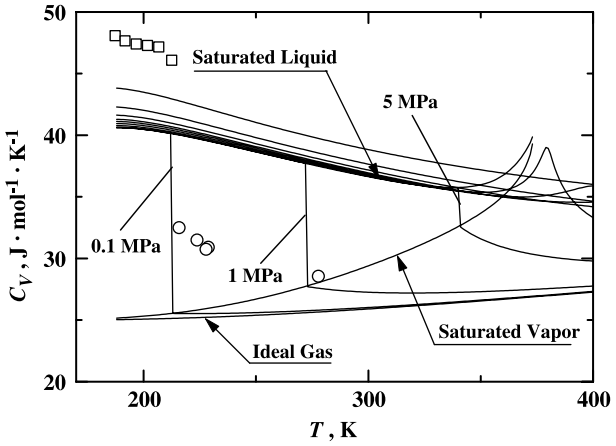

Fig. 14. Behavior of the isochoric heat-capacity calculated from the present model in the low temperature region with the available experimental data. (◯) Millar [22], (□) Swamy and Rao [24].

is $18.68\,\mathrm{kJ\cdot mol^{-1}}$; this is in good agreement with the value 18.69 ± 0.02 $\mathrm{kJ\cdot mol^{-1}}$ of Giauque and Blue [13].

$$\Delta h = T\frac{dP_S}{dT}\left(\frac{1}{\rho^V} - \frac{1}{\rho^L}\right) \tag{8}$$

where dP_S/dT is calculated from Eq. (2). The enthalpy difference between the saturated vapor enthalpy and the saturated liquid enthalpy at the normal boiling point temperature calculated by Eq. (5) is 18.63 $\mathrm{kJ\cdot mol^{-1}}$; this is smaller than the value of Giauque and Blue [13] by $0.06\,\mathrm{kJ\cdot mol^{-1}}$. Frank and Clusius [40] reported that the heat of vaporization is 19.59 kJ·

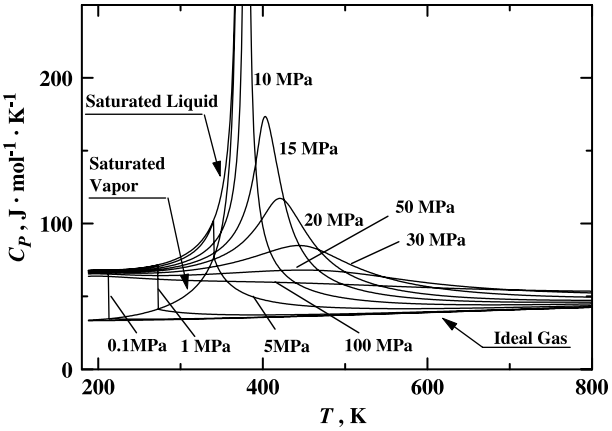

Fig. 15. Calculated isobaric heat-capacity values along isobars using the present model.

mol^{-1} at 188.7 K. The corresponding value calculated by Eq. (5) is 19.55 kJ $\cdot mol^{-1}$; this is also in good agreement with the value reported by Frank and Clusius with a deviation of 0.2%.

6. BEHAVIOR OF DERIVED THERMODYNAMIC PROPERTIES

The behavior of the isobaric heat-capacity, C_P, isochoric heat-capacity, C_V, speed-of-sound, W, and the Joule–Thomson coefficients, μ, has been calculated with the present model over an extended range of temperatures from 188 to 800 K at pressures up to 100 MPa. These results are shown in Figs. 15–18, respectively. In Fig. 18 the behavior of Joule–Thomson coefficients in the low temperature region below 350 K is also plotted. These four figures demonstrate physically reasonable behavior of the calculated values over the entire range of temperatures and pressures including the extrapolated region where no experimental data are available. These figures confirm that the present model exhibits satisfactory thermodynamic consistency over the entire fluid phase of hydrogen sulfide.

7. EXTRAPOLATION BEHAVIOR

Figure 19 shows four ideal curves, i.e., Ideal curve [Eq. (9)], Boyle curve [Eq. (10)], Joule-Thomson inversion curve [Eq. (11)], and Joule inversion curve [Eq. (12)] calculated by the present model. Melting pressures plotted in Fig. 19 were calculated by Goodwin's correlation [2]. These ideal curves are useful in assessing the behavior of the equation of

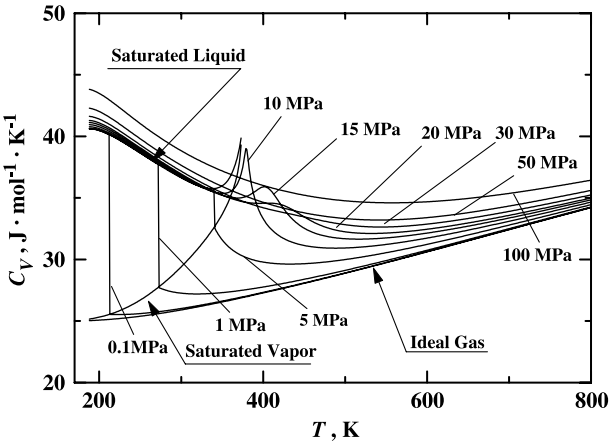

Fig. 16. Calculated isochoric heat-capacity values along isobars using the present model.

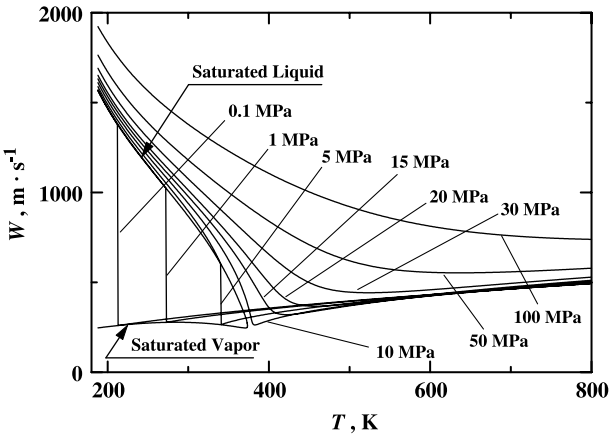

Fig. 17. Calculated speed-of-sound values along isobars using the present model.

state in the extrapolated region away from the available experimental data. The ideal curves seem to indicate reasonable behavior.

$$\left[\frac{\partial \phi^{\mathrm{r}}}{\partial \delta}\right]_{\tau} = 0 \tag{9}$$

$$\left[\frac{\partial \phi^{\mathrm{r}}}{\partial \delta}\right]_{\tau} + \delta\left[\frac{\partial^2 \phi^{\mathrm{r}}}{\partial \delta^2}\right]_{\tau} = 0 \tag{10}$$

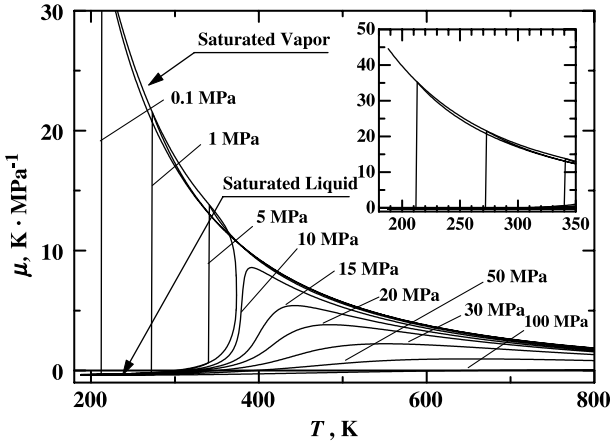

Fig. 18. Calculated Joule–Thomson coefficient values along isobars using the present model.

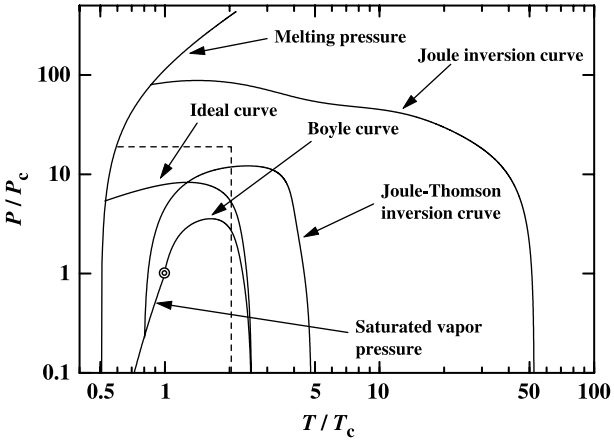

Fig. 19. Calculated ideal curves using the present model. (◎) Critical point, (- - - - - - - -) the valid region of the present model.

$$\left[\frac{\partial\phi^{\mathrm{r}}}{\partial\delta}\right]_{\tau}+\delta\left[\frac{\partial^2\phi^{\mathrm{r}}}{\partial\delta^2}\right]_{\tau}+\tau\left[\frac{\partial^2\phi^{\mathrm{r}}}{\partial\delta\partial\tau}\right]=0 \tag{11}$$

$$\left[\frac{\partial^2\phi^{\mathrm{r}}}{\partial\delta\partial\tau}\right]=0 \tag{12}$$

8. UNCERTAINTY ESTIMATION

Based on the results of comparisons between the present model and experimental data described in the previous chapter, the uncertainty in the density calculation is estimated to be 0.7% in the liquid phase and that in the pressure calculation is 0.3% in the vapor phase. The uncertainty in the vapor pressure calculation is estimated to be 0.2% and that for the isobaric heat capacity calculation is 1% in the liquid phase.

9. COMPARISON WITH EXISTING MODELS

We compared the present model with two other representative models, i.e., the Starling model [1] and the Goodwin model [2], with the aid of statistical and graphical examinations. The uncertainty and reliability of each model for $P\rho T$ data were examined statistically in terms of the absolute average deviation "AAD", the bias "BIAS", the standard deviation "SDV", the root-mean-square deviation "RMS", and the maximum percentage deviation "MAX%" with respect to each data set, and the results are summarized in Table VII. The statistical values in Table VII show that the present equation of state satisfactorily reproduces the $P\rho T$ data with deviations better than the other two models.

Figures 20 and 21 show the behavior of the isochoric heat-capacity for comparison between the existing models. The difference of the behavior of C_V is small in the vapor phase, although it is much larger in the liquid phase. The changes in the C_V values of the present model in the liquid phase are moderate, whereas those of Goodwin's model are larger, showing a minimum along the saturated liquid line at around 350 K. The isochoric heat-capacity of the Starling model is not given in his report [1]. Using C_P^0 in this study we calculated the behavior of the isochoric heat capacity from the Starling model which is shown in Fig. 21. The values of the isochoric heat capacity of the saturated liquid by the Starling model are less than those at the ideal-gas state.

10. CONCLUSION

We have developed an equation of state for hydrogen sulfide that is valid for temperatures from the triple point temperature (187.67 K) to 760 K at pressures up to 170 MPa based on selected experimental data for $P\rho T$, caloric, and saturation properties. The present model satisfactorily represents accurate experimental thermodynamic property data of hydrogen sulfide in the fluid phase. Smooth behavior of the calculated thermodynamic property values by the present model, i.e., isobaric

Table VII. Statistical Comparison of Three Different Models with $P\rho T$ Data [a]

				Present model					Goodwin model					Starling model				
Author [b]	Year	Phase	No. of data	BIAS	AAD	SDV	RMS	MAX%	BIAS	AAD	SDV	RMS	MAX%	BIAS	AAD	SDV	RMS	MAX%
Wright and Maass [4]	1931	V	54	0.05	0.08	0.09	0.10	0.26	−0.13	0.21	0.71	0.71	−4.04	−0.17	0.17	0.09	0.19	−0.43
Reamer et al. [5]	1950	V	152	0.07	0.25	0.38	0.38	1.36	−0.12	0.41	0.56	0.57	2.13	−0.48	0.66	0.87	0.99	−3.35
Lewis and Fredericks [6]	1968	V	18	−1.40	2.48	3.21	3.42	−7.79	0.10	2.99	3.73	3.63	−7.17	−3.86	3.86	2.12	4.37	−7.71
Rau and Mathia [7]	1982	V	48	1.98	3.06	3.61	4.09	11.74	3.20	3.24	2.60	4.10	11.67	−1.28	5.53	6.64	6.69	−14.39
Straty * [8]	1983	V	106	−0.05	0.10	0.26	0.26	−2.16	−0.07	0.58	0.75	0.75	1.87	−0.07	0.87	1.63	1.62	−7.35
Liu et al. [9]	1986	V	70	−1.16	1.16	0.74	1.37	−4.25	−1.25	1.67	1.63	2.04	−4.09	−1.99	1.99	1.52	2.49	−7.01
Bailey et al. [10]	1987	V	78	−0.94	1.00	0.78	1.22	−4.42	−1.08	1.24	1.32	1.70	−4.80	−1.34	1.34	1.07	1.71	−5.67
Ihmels and Gmehling [3]	2001	V	111	1.37	1.37	0.63	1.50	2.98	1.51	1.84	1.56	2.16	3.82	−0.01	1.95	2.58	2.57	−7.36
Reamer et al. [5]	1950	L	123	0.02	0.37	0.52	0.52	−2.37	−0.25	0.40	0.61	0.66	−3.12	2.77	3.11	2.79	3.93	9.89
Lewis and Fredericks [6]	1968	L	88	0.70	0.96	2.35	2.44	15.66	0.17	1.01	2.00	1.99	12.40	7.35	7.35	2.20	7.67	14.78
Rau and Mathia [7]	1982	L	19	1.20	1.70	1.41	1.83	−3.33	0.55	1.09	1.16	1.26	−3.31	9.82	9.82	3.23	10.31	13.44
Straty [8]	1983	L	6	0.82	0.99	0.69	1.03	1.47	−1.25	1.25	0.58	1.36	−2.00	8.34	8.34	0.90	8.38	9.60
Liu et al. [9]	1986	L	36	3.05	3.06	2.29	3.79	7.02	2.03	2.76	2.55	3.23	6.33	9.83	9.83	3.25	10.34	16.18
Bailey et al. [10]	1987	L	8	2.74	2.81	2.67	3.71	7.09	1.49	2.50	3.08	3.24	6.43	7.39	8.67	6.41	9.52	16.26
Ihmels and Gmehling * [3]	2001	L	357	−0.31	0.34	0.88	0.93	−11.09	−0.69	0.69	1.08	1.28	−12.41	3.25	3.46	3.26	4.60	−14.89

[a] Note that deviations of PρT data are given with respect to densities in the liquid phase, whereas with respect to pressures in the vapor phase.

[b] Data used as input data are denoted by *.

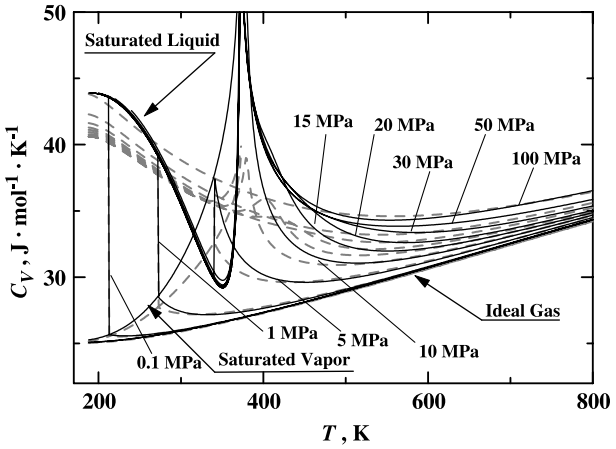

Fig. 20. Comparison of calculated isochoric heat-capacity values along isobars between the Goodwin model and the present model. (———) Goodwin model [2], (- - - - - - - -) the present model.

heat-capacity, isochoric heat capacity, speed-of-sound, Joule–Thomson coefficients, Ideal curve, Boyle curve, Joule–Thomson inversion curve, and Joule inversion curve confirms not only the thermodynamic consistency of the present model but also its range of validity.

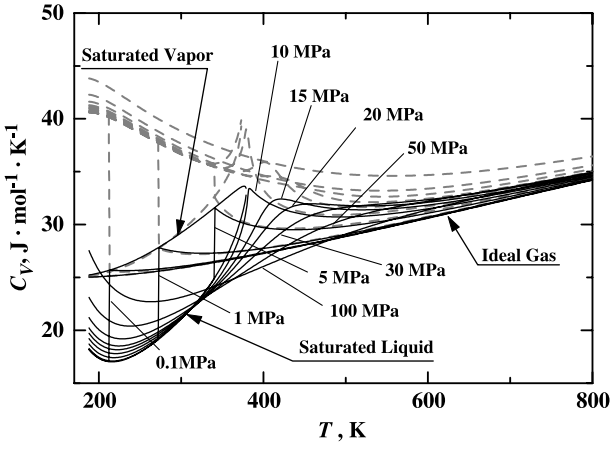

Fig. 21. Comparison of calculated isochoric heat-capacity values along isobars between the Starling model and the present model. (———) Starling model [1], (- - - - - - - -) the present model.

REFERENCES

1. K. E. Starling, *Fluid Thermodynamic Properties for Light Petroleum Systems* (Gulf Publishing Co., Houston, Texas, 1973).
2. R. D. Goodwin, *Hydrogen Sulfide Provisional Thermophysical Properties from 188 to 700* K *at Pressures to 75* MPa, NBSIR 83-1694, Nat. Bureau Stds., Boulder, Colorado (1983).
3. E. C. Ihmels and J. Gmehling, *Ind. Eng. Chem. Res.* **40**:4470 (2001).
4. R. H. Wright and O. Maass, *Can. J. Res.* **5B**:442 (1931).
5. H. H. Reamer, B. H. Sage, and W. N. Lacey, *Ind. Eng. Chem.* **42**:140 (1950).
6. L. C. Lewis and W. J. Fredericks, *J. Chem. Eng. Data* **13**:482 (1968).
7. H. Rau and W. Mathia, *Ber. Bunsenges. Phys. Chem.* **86**:108 (1982).
8. G. C. Straty: cited as Ref. 43 in Ref. 2.
9. C. H. Liu, D. M. Bailey, J. C. Holste, P. T. Eubank, and K. R. Hall, *Hydrocarbon Process.* **65**:41 (1986).
10. D. M. Bailey, C. H. Liu, J. C. Holste, K. R. Hall, P. T. Eubank, and K. M. Marsh, GPA Research Report 107, Gas Processors Assoc., Tulsa, Oklahoma (1987).
11. E. Cardoso, *Gazz. Chim. Ital.* **51**:153 (1921).
12. A. Klemenc and O. Bankowski, *Z. Anorg. Chem.* **208**:348 (1932).
13. W. F. Giauque and R. W. Blue, *J. Am. Chem. Soc.* **58**:831 (1936).
14. A. M. Clark, A. H. Cockett, and H. S. Eisner, *Proc. Roy. Soc. Lond. Ser. A* **209**:408 (1951).
15. J. A. Bierlein and W. B. Kay, *Ind. Eng. Chem.* **45**:618 (1953).
16. W. B. Kay and D. B. Brice, *Ind. Eng. Chem.* **45**:615 (1953).
17. W. B. Kay and G. M. Rambosek, *Ind. Eng. Chem.* **45**:221 (1953).
18. H. H. Reamer, B. H. Sage, and W. N. Lacey, *Ind. Eng. Chem.* **45**:1805 (1953).
19. E. C. W. Clarke and D. N. Glew, *Can. J. Chem.* **48**:764 (1970).
20. J. P. Baxter, L. J. Burrage, and C. C. Tanner, *J. Soc. Chem. Ind.* **53**:410 (1934).
21. A. G. Cubitt, C. Henderson, L. A. K. Staveley, I. M. A. Fonseca, A. G. M. Ferreira, and L. Q. Lobo, *J. Chem. Thermodyn.* **19**:703 (1987).
22. R. W. Millar, *J. Am. Chem. Soc.* **45**:874 (1923).
23. K. Clusius and A. Frank, *Z. Phys. Chem.* **34B**:420 (1936).
24. K. N. Swamy and R.V. G. Rao, *Z. Phys. Chem.* **71**:218 (1970).
25. W. F. Giauque and J. O. Clayton, *J. Am. Chem. Soc.* **55**:4875 (1933).
26. R. Span, E. W. Lemmon, R. T. Jacobsen, W. Wagner, and A. Yokozeki, *J. Phys. Chem. Ref. Data* **29**:1361 (2000).
27. P. C. Cross, *J. Chem. Phys.* **3**:168 (1935).
28. W. A. Felsing and G. W. Drake, *J. Am. Chem. Soc.* **58**:1714 (1936).
29. G. M. Barrow and K. S. Pitzer, *Ind. Eng. Chem.* **41**:2737 (1949).
30. W. H. Evans and D. D. Wagman, *J. Res. Natl. Bur. Stand.* **49**:141 (1952).
31. B. J. McBride and S. Gordon, *J. Chem. Phys.* **35**:2198 (1961).
32. H. D. Baehr, H. Hartmann, H. C. Pohl, and H. Schomäcker, *Thermodynamic Functions of Ideal Gases for Temperatures up to 6000* K (Thermodynamische Funktionen idealer Gase für Temperaturen bis 6000 K) (Springer, Berlin, 1968).
33. JANAF, Thermodynamic Tables, 3rd. Ed., M. W. Chase, J. L. Curnutt, J. R. Downey, R. A. McDonald, A. N. Syverud, and E. A. Valenzuela, *J. Phys. Chem. Ref. Data* **14**: (Suppl. 1): (1985).
34. TRC, *Thermodynamic Tables* (Thermodynamic Research Center, Texas A & M University, College Station, Texas, 1972–1993).
35. M. Jaeschke and P. Schley, *Int. J. Thermophys.* **16**:1381 (1995).

36. E. Cardoso and E. Arni, *J. Chim. Phys.* **10**:504 (1912).
37. F. Y. Jou, J. J. Carroll, and A. E. Mather, *Fluid Phase Equilibr.* **109**:235 (1995).
38. P. Guilbot, P. Th′eveneau, A. Baba-Ahmed, S. Horstmann, K. Fischer, and D. Richon, *Fluid Phase Equilib.* **170**:193 (2000).
39. P. J. Mohr and B. N. Taylor, *J. Phys. Chem. Ref. Data* **28**:1713 (1999).
40. A. Frank and K. Clusius, *Z. Phys. Chem.* **B42**:395 (1939).